Bull. Mater. Sci., Vol. 35, No. 5, October 2012, pp. 801–809. © Indian Academy of Sciences.

Preparation, characterization and photocatalytic activity of TiO_2/polyaniline core-shell nanocomposite

ALI OLAD*, SEPIDEH BEHBOUDI and ALI AKBAR ENTEZAMI†
Department of Applied Chemistry, Faculty of Chemistry, University of Tabriz, Tabriz, Iran
†Department of Organic Chemistry, Faculty of Chemistry, University of Tabriz, Tabriz, Iran

MS received 17 September 2011; revised 24 October 2011

Abstract. **Polyaniline (PANI) as a promising conducting polymer has been used to prepare polyaniline/TiO_2 (PANI/TiO_2) nanocomposite with core-shell structure as photocatalyst. Titanium dioxide (TiO_2) nanoparticles with an average crystal size of 21 nm were encapsulated by PANI via the *in situ* polymerization of aniline on the surface of TiO_2 nanoparticles. FT–IR, UV-Vis-NIR, XRD, SEM and TEM techniques were used to characterize the PANI/TiO_2 core-shell nanocomposite. Photocatalytic activity of PANI/TiO_2 nanocomposite was investigated under both UV and visible light irradiations and compared with unmodified TiO_2 nanoparticles. Results indicated deposition of PANI on the surface of TiO_2 nanoparticles which improved the photocatalytic activity of pristine TiO_2 nanoparticles.**

Keywords. **Photocatalyst; TiO_2 nanoparticle; polyaniline; conducting polymer; core-shell nanocomposite.**

1. Introduction

In recent years, conducting polymer/inorganic hybrid materials have been extensively studied because of their synergetic effects and potential applications in chemistry, physics, electronic, optics and biotechnology (Wang and Zeng 2009a,b; Xiong *et al* 2010). The physical and chemical properties of final conducting polymer/inorganic composite can be tuned through proper selection of conducting polymer type and inorganic material for particular purposes. Titanium dioxide (TiO_2) due to the advantages of high chemical stability, high photocatalytic activity, relatively low cost and nontoxicity, is one of the most important photoactive reagents which are widely used for degradation of air and water organic pollutants (Dey *et al* 2004; Wang *et al* 2010). TiO_2 acts as a photocatalyst in advanced oxidation processes (AOPs) by generation of reactive $OH^{\cdot}$ radicals. The $OH^{\cdot}$ radicals can oxidize a broad range of organic pollutants (Mishra and Srivastava 2008; Salem *et al* 2009; Polyakov *et al* 2010). However, TiO_2 due to its wide bandgap (3·2 eV), can only be photoactive under UV light ($\lambda < 366$ nm) which has carcinogenic effect and occupies small fraction (3–5%) of solar photons (Li *et al* 2008a,b; Narayana *et al* 2011). Also relatively high recombination rate of electron–hole pairs in excited TiO_2 restricts its photocatalytic activity (Min *et al* 2007). Various attempts have been made to extend the photoresponse region of TiO_2 towards visible light and increase its photocatalytic efficiency under UV and visible light irradiations (Zhu *et al* 2010). Doping of TiO_2 by metals (Sakthivel *et al* 2004), and non-metals (Lu *et al* 2007), deposition of noble metals on the surface of TiO_2 (Li and Li 2001), composition of TiO_2 with narrow bandgap semiconductors (Li *et al* 2009) and surface dye sensitization of TiO_2 (Sun and Xu 2009), are the most common methods which have been used to improve photocatalytic performance of TiO_2. Although, among these methods dye sensitization is a promising method to improve the photoactivity of TiO_2 under visible light region, but it suffers from dissolution and photocatalytic degradation of the dyes (Min *et al* 2007). Conducting polymers with extended π-conjugated electron system and good environmental stability act as stable photo-sensitizer to sensitize TiO_2 by the absorption of a broad spectrum of ultraviolet and visible light (190–800 nm) irradiations (Wang and Min 2007; Wang *et al* 2009). Among conducting polymers PANI is a good candidate due to its high stability, low cost, high charge (electron-hole) carrying efficiency and ease of synthesis (Wang and Min 2007; Olad and Rashidzadeh 2008; Olad and Naseri 2010). TiO_2 is a typical *n*-type semiconductor and PANI is usually considered as a *p*-type conducting polymer (Shi *et al* 2009; Zhu *et al* 2010). Thus their combination brings a good capacitive material with good conductivity and stability (Ganesan and Gedanken 2008). There are several reports on the preparation, investigation of properties (Somani *et al* 1999; Li *et al* 2004, 2006; Yavuz and Gok 2007) and applications of PANI/TiO_2 composite materials (Zhang *et al* 2006; Sathiyanarayanan *et al* 2007; Lokesh *et al* 2008). Studies on the surface and interface properties of PANI/TiO_2 have indicated that a nanocomposite at the molecular level has been created (Somani *et al* 1999; Li *et al* 2003). Previous researchers have shown that properties of PANI/TiO_2 composites are quite different from pure PANI or TiO_2, which is due to the existence of strong interaction between two components (Nagaraja *et al* 2009; Kim *et al* 2009). The

*Author for correspondence (a.olad@yahoo.com)

synthesis method has a great effect on the final properties of PANI/TiO_2 composite (Xu *et al* 2005; Shi *et al* 2009; Karim *et al* 2009). Various methods such as ultrasonic irradiation, *in situ* polymerization, self assembly method, graft polymerization and UV curable polymerization methods have been used to prepare PANI/TiO_2 composite systems (Li *et al* 2006; Kim *et al* 2009). *In situ* polymerization of aniline in the presence of TiO_2 nanoparticles has been used commonly for preparation of PANI/TiO_2 nanocomposites (Xu *et al* 2005; Zhang *et al* 2005, 2006; Yavuz and Gok 2007). In addition to TiO_2 with established photocatalytic behaviour (Chen and Liu 2007), conjugated polymers were also used for photocatalysis (Muktha *et al* 2007). The photosensitizing effect of PANI on TiO_2 has been reported. The application of a conducting polymer such as PANI expands the photoactive region of TiO_2 toward visible light irradiation (Min *et al* 2007; Wang and Min 2007; Li *et al* 2008a,b). Many efforts have been made to improve photocatalytic activity of the PANI/TiO_2 system (Wang and Zeng 2009a,b; Liao *et al* 2011). The application of PANI/TiO_2 as a photocatalyst for the photodegradation of environmental pollutants has been investigated in literature (Li *et al* 2008a,b; Salem *et al* 2009). Liu and Guo (1991) used the hybrid of PANI and TiO_2 for photocatalytic removal of phenol from water. The synergetic effects of PANI and TiO_2 in photocatalytic degradation of colourful water contaminants under visible light irradiation have been demonstrated (Zhang *et al* 2008; Wang *et al* 2010; Liao *et al* 2011). In this study, the PANI/TiO_2 core-shell nanocomposite was prepared using *in situ* polymerization method and then photocatalytic degradation of methyl orange (MeO) in the presence of low amount of PANI/TiO_2 nanocomposite as photocatalyst was investigated.

2. Experimental

2.1 *Materials and reagents*

Aniline monomer (Merck Company, Germany) was distilled two times under vacuum and stored below 4 °C prior to use. TiO_2 nanoparticles (Degussa P25, average crystal size, 21 nm) were used to prepare PANI/TiO_2 nanocomposite. All other reagents including ammonium peroxodisulfate (APS, $(NH_4)_2S_2O_8$), hydrochloric acid (HCl) and methyl orange (MeO), were purchased from Merck Company as analytical grade and were used as received.

2.2 *Preparation of PANI/TiO_2 core-shell nanocomposite*

PANI/TiO_2 nanocomposite was prepared as follows: TiO_2 nanoparticles (1 g) were dispersed in 190 ml of HCl aqueous solution (1·21 M) containing 0·3 ml aniline under ultrasonic vibration to reduce the aggregation of TiO_2 nanoparticles. APS (0·863 g) was dissolved in 15 ml of HCl aqueous solution (1·21 M) and added drop wise into the solution containing aniline monomer under constant stirring. The mixture was allowed to polymerize under stirring for 5 h at room temperature. Reaction mixture was filtered under vacuum and washed with ethanol and water and then dried at 60 °C for 24 h to obtain PANI emeraldine salt (ES) as a green powder.

2.3 *Instruments*

Fourier–transform infrared (FT–IR) spectra of HCl-doped PANI and PANI/TiO_2 nanocomposite were obtained by using a Bruker Tensor 27 spectrometer. Morphology of samples was observed on a Cam scan MV 2300 scanning electron microscope (SEM) and a Philips-CM10 transmission electron microscope (TEM) with an accelerating voltage of 100 kV. X-ray diffraction (XRD) patterns were taken on a Siemens D5000 X-ray diffractometer with a Cu Kα X-ray radiation ($\lambda = 0{\cdot}154$ nm). A Shimadzu UV-1700 Farma spectrophotometer was used to record the UV-Vis-near IR spectra of samples and degradation measurement of MeO solutions.

2.4 *Evaluation of photocatalysis*

The photocatalytic activity of pristine TiO_2 and PANI/TiO_2 nanocomposite was evaluated by determining the decolourization efficiency and rate constant of MeO photodegradation. The aqueous solutions of MeO were used as model pollutant for investigation of the photocatalytic activity of samples. 0·01 g of pristine TiO_2 or PANI/TiO_2 photocatalysts was added to 50 ml of MeO aqueous solution (10 mg·L^{-1}) under magnetic stirring. The solid concentration in final suspension was 200 mg·L^{-1}. The suspension was stirred in dark condition at room temperature (25 °C) for 30 min to achieve adsorption equilibrium for MeO. Afterward, the suspension was illuminated by a 50 W linear halogen lamp equipped with UVA absorbent filter ($\lambda > 400$ nm) for 120 min. Samples for monitoring of remaining MeO concentration in aqueous solution were drawn out by a syringe equipped with 2·5 μm pore size filter at various time intervals of photocatalytic degradation reaction. Concentration of remaining MeO was obtained by measuring the absorbance of samples at $\lambda_{max} = 464$ nm with a UV-Vis spectrophotometer. The determined absorption was converted to concentration through the standard calibration curve (figure 1). Also figure 2 shows UV-Vis absorption spectrum of MeO aqueous solution. In the next step, same experiments were repeated exactly with 30 W UV tube lamp (length, 41 cm, diameter, 2·5 cm). The photocatalytic degradation efficiency was calculated using (1).

$$R\% = \frac{C_0 - C_t}{C_0} \times 100, \tag{1}$$

where $R\%$ is degradation efficiency of MeO, C_0 the initial concentration of MeO in aqueous solution and C_t the concentration of MeO in aqueous solution at different reaction time, t (Min *et al* 2007; Zhu *et al* 2010).

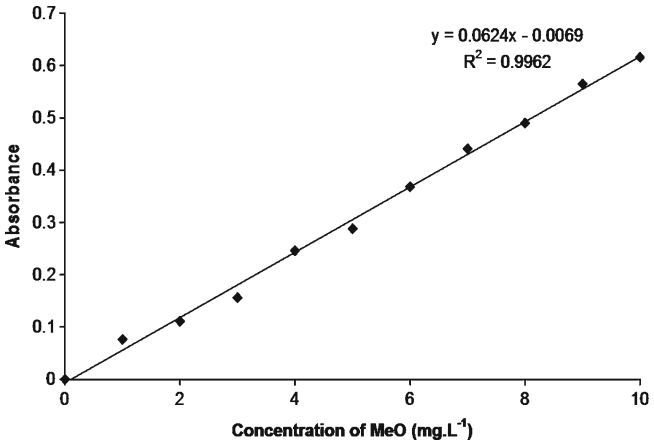

Figure 1. Calibration curve of MeO in $\lambda_{max} = 464$ nm.

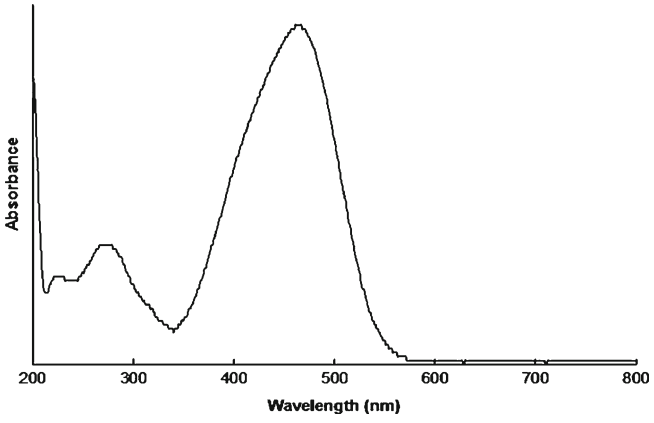

Figure 2. UV-Vis absorption spectrum of MeO aqueous solution (1 ppm).

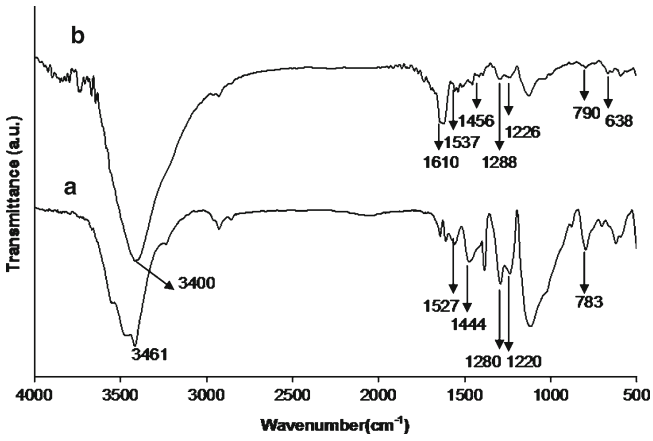

Figure 3. FT–IR spectra of HCl-doped PANI (**a**) and PANI/TiO_2 nanocomposite (**b**).

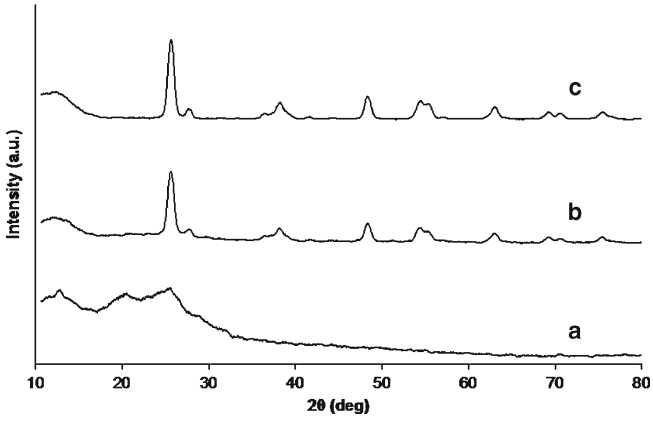

Figure 4. XRD patterns of pure HCl-doped PANI (**a**), PANI/TiO_2 nanocomposite (**b**) and pristine TiO_2 nanoparticles (**c**).

3. Results and discussion

3.1 *FT–IR spectra*

Fourier transform–infrared (FT–IR) spectroscopy was used to characterize the prepared PANI/TiO_2 nanocomposite. Figure 3 shows FT–IR spectra of HCl-doped PANI (figure 3a) and PANI/TiO_2 nanocomposite (figure 3b). According to figure 3a, the main characteristic peaks of HCl-doped PANI appeared at 3461, 1527, 1444, 1280, 1220 and 783 cm^{-1}. The peak at 3461 cm^{-1} is attributed to the stretching mode of N–H band. C=N and C=C stretching modes of the quinoid and benzenoid units occur at 1527 cm^{-1} and 1444 cm^{-1}, respectively, while the band at 1280 cm^{-1} is attributed to the C–N stretching mode of the benzenoid unit. The band at 1087 cm^{-1} is due to quinoid unit of HCl-doped PANI and the peak at 783 cm^{-1} is associated with the C–C and C–H bands of benzenoid unit (Kim *et al* 2009). Figure 3b reveals main characteristic peaks of HCl-doped PANI appearing in the FT–IR spectrum of PANI/TiO_2 nanocomposite, which are 3400, 1610, 1537, 1456, 1288, 1226 and 790 cm^{-1}, respectively. Also, the characteristic peak of TiO_2 (638 cm^{-1}) appeared at the FT–IR spectrum of PANI/TiO_2 nanocomposite. The shift of the PANI/TiO_2 nanocomposite characteristic peaks toward higher values and appearance of a new peak (1610 cm^{-1}) in the FT–IR spectrum of PANI/TiO_2, indicate a strong interaction that was created at the interface of PANI and TiO_2 in the PANI/TiO_2 nanocomposite. When APS as oxidant is added to the reaction system, PANI formation proceeds initially on the surface of TiO_2 and a shell of PANI is formed on the surface of TiO_2 nanoparticles. It leads to the high adhesion of PANI chains to the surface of TiO_2 nanoparticles (Min *et al* 2007). Also titanium as a transition metal element has intense tendency to form coordination compounds with nitrogen atom in PANI molecules. Simultaneously, hydrogen bonding can occur between PANI and TiO_2 nanoparticles (Li *et al* 2008b). Therefore, a nanocomposite at molecular level was formed.

3.2 *X-ray diffraction patterns*

Figure 4 shows X-ray diffraction (XRD) patterns of pristine TiO_2 nanoparticles, HCl-doped PANI and PANI/TiO_2

nanocomposite. Figure 4a reveals that PANI also has some degree of crystallinity. A broad peak around $2\theta = 25^\circ$ in XRD pattern of HCl-doped PANI may be attributed to the scattering from PANI chains at interplanar spacing (Li *et al* 2004). Figure 4b shows appearance of peaks in XRD pattern of pristine TiO_2 nanoparticles which can be indexed as the anatase polymorph of TiO_2 (Dong *et al* 2010). Also figures 4b and c show that there is no difference between XRD pattern of PANI/TiO_2 core-shell nanocomposite and XRD pattern of pristine TiO_2 nanoparticles, which reveals deposition of PANI on the surface of TiO_2 nanoparticles which has no effect on the crystallinity of TiO_2 nanoparticles. Therefore, the polymorph of TiO_2 in the PANI/TiO_2 nanocomposite is still anatase. However, PANI peaks in the PANI/TiO_2 core-shell nanocomposite are not detected. This result suggested that the crystallization of PANI molecular chain has been hampered in PANI/TiO_2 nanocomposite (Lai *et al* 2011). This is because when PANI chains are adsorbed on the surface of TiO_2 nanoparticles, due to the restrictive effect of TiO_2 nanoparticles crystallinity of PANI is compromised (Xia and Wang 2002). The crystallite size of pure TiO_2 nanoparticles and core-shell PANI/TiO_2 nanocomposite was calculated to be 21·2 nm and 25·7 nm, respectively according to the Debye–Scherrer formula (2):

$$D = \frac{0{\cdot}89\lambda}{\beta \cos\theta}, \tag{2}$$

where D is the average crystallite size (Å), λ the wavelength of X-ray radiation (Cu Kα), β the full width at half maximum (FWHM) intensity of the peak and θ the Bragg diffraction angle (Pourata *et al* 2009). Calculated crystallite sizes of pure TiO_2 nanoparticles and PANI/TiO_2 core-shell nanocomposite indicate that the thickness of PANI shell on the surface of TiO_2 nanoparticles in PANI/TiO_2 core-shell nanocomposite is ~5 nm, which is consistent with TEM results.

3.3 *Morphological studies*

The surface morphology and surface area are very effective parameters in photocatalytic activity of TiO_2 nanoparticles. TiO_2 nanoparticles due to the high surface energy tend to be aggregated. This agglomeration deteriorates the photocatalytic activity through the reduction of effective surface area of TiO_2 nanoparticles. Therefore, investigation of the surface area and morphology of pristine TiO_2 nanoparticles and PANI/TiO_2 nanocomposite as photocatalyst is vital. Figure 5 shows scanning electron micrographs (SEM) of pristine TiO_2 (figure 5a) and PANI/TiO_2 nanocomposite (figure 5b). Results show more agglomeration of pristine TiO_2 nanoparticles while TiO_2 nanoparticles modified by PANI (PANI/TiO_2 nanocomposite) are in more separated state. This could be due to the formation of PANI shell on the surface of TiO_2 nanoparticles which causes repulsion forces between nanoparticles and prevents their agglomeration (Li *et al* 2008b). According to the UV-Vis

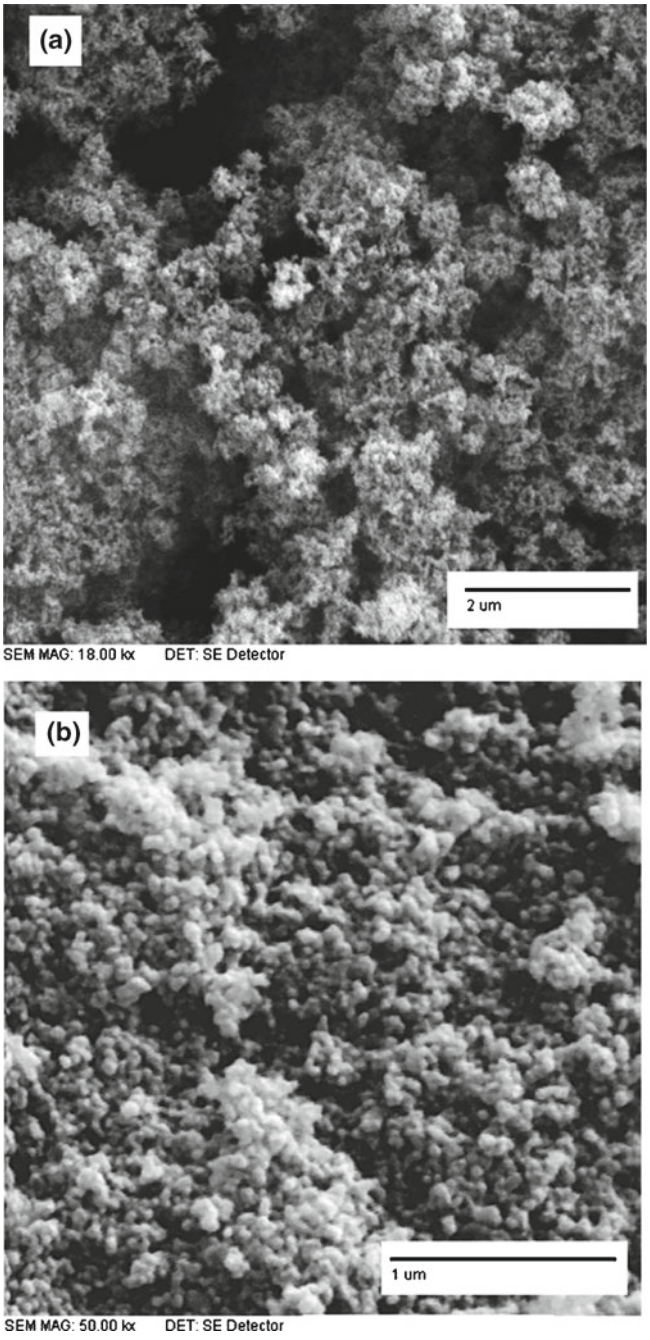

Figure 5. SEM micrographs of (**a**) pristine TiO_2 nanoparticles and (**b**) PANI/TiO_2 nanocomposite.

spectroscopy results which will be noted in § 3.5, PANI in ES form which encapsulates TiO_2 nanoparticles is positively charged, resulting in repulsion hence minimizing agglomeration of TiO_2 nanoparticles (Kim *et al* 2009). Figure 6 shows transmission electron micrographs (TEM) of pristine TiO_2 nanoparticles (figure 6a) and PANI/TiO_2 nanocomposite (figure 6b). Figure 6 reveals pristine TiO_2 nanoparticles are highly agglomerated while this agglomeration in PANI/TiO_2 nanocomposite decreased considerably. Figure 6b presents

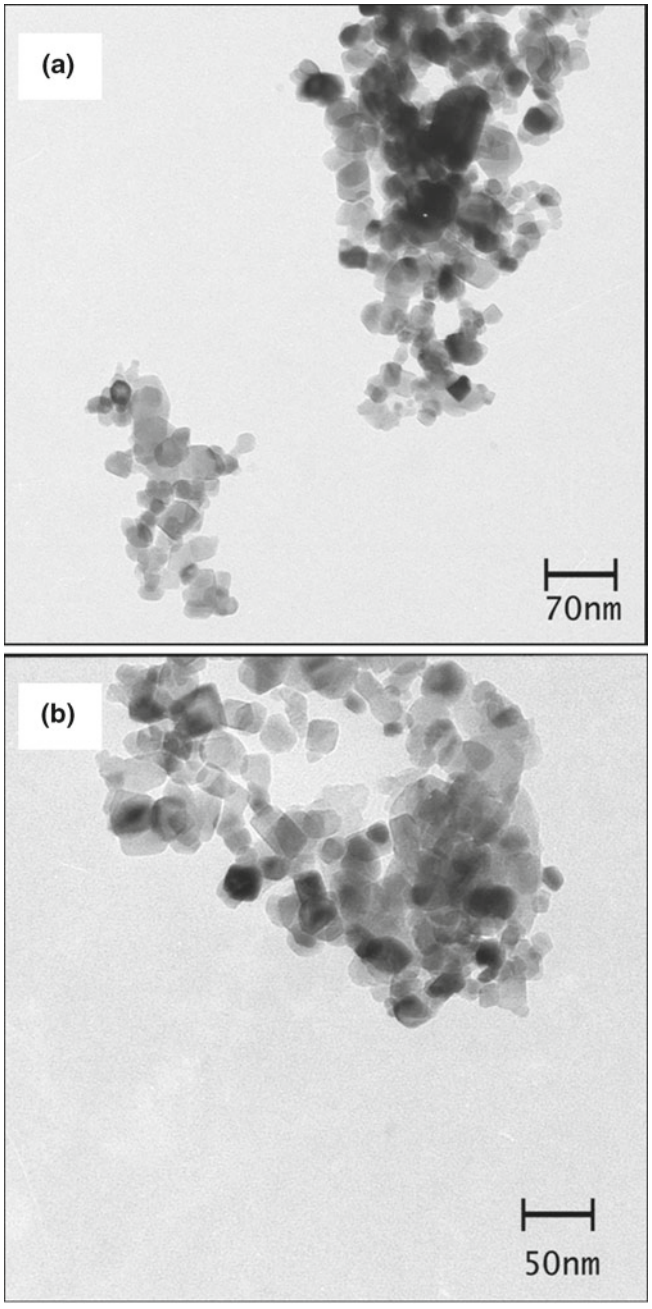

Figure 6. TEM images of (**a**) pristine TiO_2 nanoparticles and (**b**) PANI/TiO_2 nanocomposite.

that PANI/TiO_2 nanocomposite possesses a core-shell structure. Therefore, a core-shell structure has been formed by the *in situ* polymerization of aniline on the surface of TiO_2 nanoparticles.

3.4 *Formation mechanism of core-shell PANI/TiO_2 nanocomposite*

It has been well known that TiO_2 nanoparticles have zero charge point at pH = 6. Therefore, they are positively charged in acidic solution required for the *in situ* polymerization of aniline as indicated by (3) (Kosmulski 2002; Chen and Cao 2006; Salem *et al* 2009).

$$TiOH + H^+ \leftrightarrow TiOH_2^+. \quad (3)$$

Figure 7 illustrates the formation mechanism of core-shell PANI/TiO_2 nanocomposite. Chloride anions are adsorbed on the positively charged surface of TiO_2 nanoparticles to neutralize the created positive charge on the surface of TiO_2 nanoparticles. Aniline monomer in acidic solution (HCl) is transformed to the anilinium cation. Therefore, electrostatic interaction occurred between chloride anions adsorbed on the surface of TiO_2 nanoparticles and anilinium monomers, which are available in reaction media. Polymerization of anilinium cations, causes formation of PANI shell around the TiO_2 nanoparticles. This mechanism suggests the formation of PANI/TiO_2 nanocomposite with core-shell structure which is highly probable by the modification of TiO_2 nanoparticles via the *in situ* polymerization of aniline. Results obtained by SEM and TEM micrographs are in good agreement with the proposed mechanism (Li *et al* 2008b).

3.5 *Light absorption characteristics of photocatalysts*

The absorption of light energy is the basis of TiO_2 photocatalytic activity. To understand the effect of PANI on the light absorption characteristics of TiO_2 nanoparticles, UV-Vis-NIR spectra of samples were recorded (figure 8). UV-Vis-NIR spectrum of PANI/TiO_2 nanocomposite shows the absorption peaks at 228, 332, 460 and 790 nm. The peak at 228 nm was attributed to TiO_2 comprising the core of PANI/TiO_2 core-shell nanocomposite. The peak observed at 332 nm is corresponding to $\pi \rightarrow \pi^*$ transition or exciton transition. Two broad absorption peaks at 460 and 790 nm should be assigned to the polaron-π^* and π-polaron transition from the charged cationic species in the PANI ES state (Kim *et al* 2009). As shown in figure 8, the PANI/TiO_2 nanocomposite exhibits different optical behaviour from that observed for pristine TiO_2 nanoparticles. PANI/TiO_2 nanocomposite not only absorbs the UV light but also significantly absorb the visible and near-IR (figure 8b). Whereas pristine TiO_2 nanoparticles absorb only the UV region and a small part of visible light (figure 8a). These results indicate that PANI is a good sensitizer for TiO_2 nanoparticles and increases the photoactive region of TiO_2 nanoparticles through the absorption of visible and near-IR lights (Wang and Min 2007).

3.6 *Photocatalytic activities of pristine and modified TiO_2 nanoparticles*

The photocatalytic activity of pristine TiO_2 and PANI/TiO_2 nanocomposite was evaluated under UV and visible light irradiations. The photocatalytic degradation efficiency of

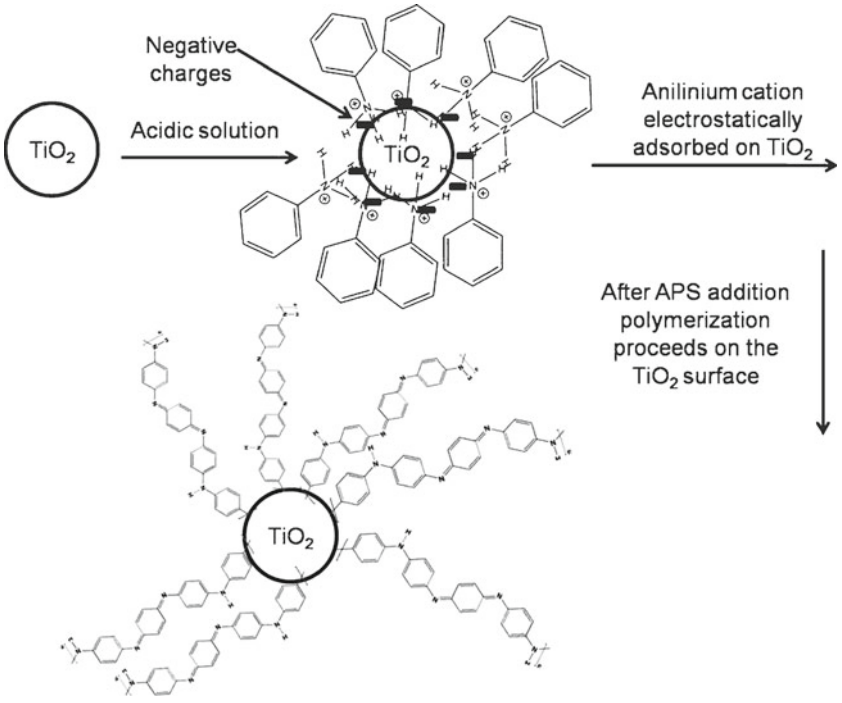

Figure 7. Formation scheme of PANI/TiO_2 core-shell nanocomposite.

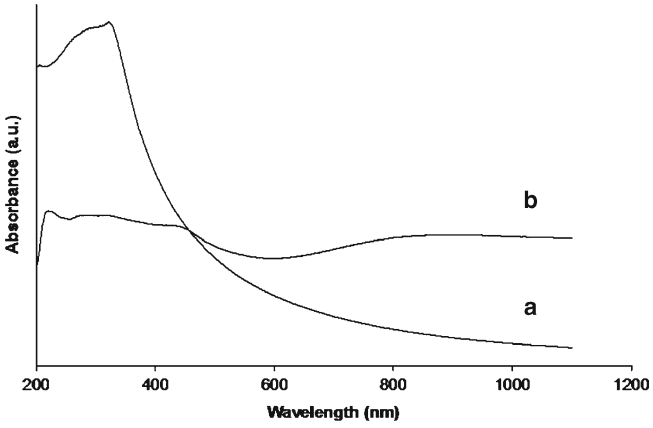

Figure 8. UV-Vis-NIR spectra of pristine TiO_2 nanoparticles (**a**) and PANI/TiO_2 nanocomposite (**b**).

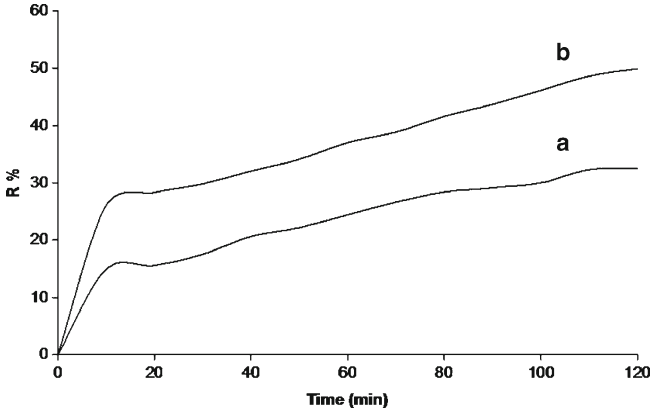

Figure 9. Degradation efficiency of MeO during 120 min illumination under visible light using pristine TiO_2 (**a**) and PANI/TiO_2 nanocomposite (**b**) as photocatalyst.

MeO in the presence of pristine TiO_2 and PANI/TiO_2 nanocomposite was obtained according to the procedure described § 2. Figure 9 shows photodegradation efficiency of MeO in the presence of TiO_2 and PANI/TiO_2 nanocomposite photocatalysts under visible light irradiation against contact time. Figure 9 indicates photodegradation efficiency of MeO in the presence of PANI/TiO_2 nanocomposite as photocatalyst is significantly higher than pristine TiO_2 nanoparticles. The kinetic plots for MeO degradation with pristine TiO_2 and PANI/TiO_2 nanocomposite photocatalysts under visible light illumination are shown by pseudo-first order reaction (Li *et al* 2008a,b; Wang and Zeng 2009a; Wang *et al* 2010; Liao *et al* 2010) in figure 10. This model is described by (4).

$$-\ln(C_t/C_0) = k_{app}t, \tag{4}$$

where k_{app} is the apparent rate constant, C_0 the initial concentration of MeO and C_t the concentration of MeO at various contact times, t.

Half time of MeO photodegradation was calculated using (5) which was derived from (4) by replacing C_t with $C_0/2$ (Dong *et al* 2010):

$$t_{1/2} = \ln 2/k = 0{\cdot}6931/k_{app}, \tag{5}$$

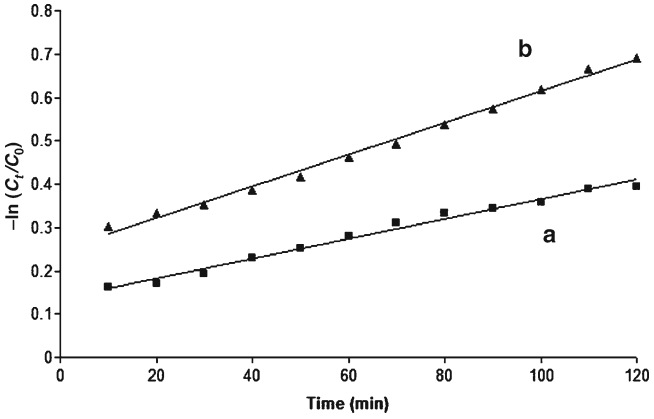

Figure 10. Kinetics plots for linear fitting of data obtained from pseudo-first-order reaction model for MeO degradation under visible light irradiation using pristine TiO_2 (**a**) and PANI/TiO_2 (**b**) as photocatalyst.

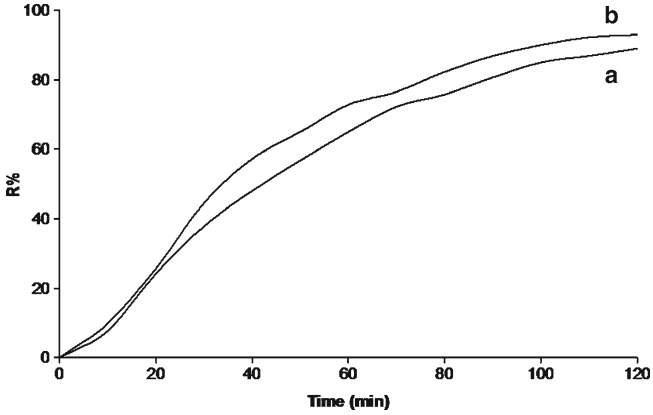

Figure 11. Degradation efficiency of MeO during 120 min illumination under UV light using pristine TiO_2 (**a**) and PANI/TiO_2 nanocomposite (**b**) as photocatalyst.

Table 1. Apparent rate constants (k_{app}), linear regression coefficients, half time of MeO photodegradation from a plot of $-\ln(C_t/C_0) = k_{app}t$ and degradation efficiency (%) of MeO after 120 min illumination under visible light.

Photocatalyst	Degradation efficiency (%)	R^2	k_{app} (min^{-1})	$t_{1/2}$ (min)
Neat TiO_2	32·5	0·993	0·0023	301·35
PANI/TiO_2	49·9	0·985	0·0037	187·32

The determined pseudo-first-order rate constants (k_{app}), linear regression coefficients (R^2), degradation efficiency and half time of MeO photodegradation after 120 min illumination are presented in table 1. From table 1, it can be seen that the deposition of PANI shell on the surface of TiO_2 nanoparticles improves apparent rate constant and half time of MeO degradation compared to pristine nano-TiO_2 photocatalyst. Figure 11 shows photodegradation efficiency of MeO against contact time with TiO_2 and PANI/TiO_2 photocatalysts under UV irradiation. Figure 11 indicates degradation efficiency of MeO in the presence of PANI/TiO_2 nanocomposite which is higher than pristine TiO_2 nanoparticles. The kinetic plots of MeO degradation with PANI/TiO_2 and pristine TiO_2 photocatalysts under UV light illumination are shown in figure 12. Also apparent rate constants, regression coefficients, degradation efficiency and half time of MeO photodegradation under UV illumination are tabulated in table 2. One of the possible reasons for the improvement of PANI/TiO_2 photocatalytic activity under both UV and visible light illuminations is the reduced aggregation state of TiO_2 nanoparticles in PANI/TiO_2 nanocomposite. This leads to the higher specific surface area and higher interaction between PANI/TiO_2 photocatalyst and dye aqueous solution compared to pristine TiO_2 nanoparticles (Li *et al* 2008a,b). Therefore, adsorption of dye molecules on the nanocomposite is higher than pristine TiO_2 nanoparticles.

Both PANI and TiO_2 nanoparticles absorb photons at their interface under irradiation. Since the CB of TiO_2 and lowest unoccupied molecular orbital (LUMO) of PANI are well matched for the charge transfer, the electrons generated by PANI $\pi \rightarrow \pi^*$ transition under visible light illumination can be injected into the CB of TiO_2 and the electrons in the VB of TiO_2 are delivered to PANI layer (Wang and Min 2007). While under UV light illumination photogenerated holes in the VB of TiO_2 can be transferred directly to highest unoccupied molecular orbital (HOMO) of PANI, as the VB of TiO_2 matches well with the HOMO of PANI (Zhang *et al* 2008). Subsequently the photogenerated electron–hole pairs in the PANI/TiO_2 photocatalyst interface can be transferred to the surface, which reacts directly with adsorbed MeO molecules on the surface of PANI/TiO_2 nanocomposite or indirectly decompose MeO through the production of $OH^{\cdot}$ radicals (Salem *et al* 2009). Therefore, charge separation enhancement in PANI/TiO_2 nanocomposite interface causes improvement of photocatalytic activity of PANI/TiO_2 nanocomposite under both UV and visible light illuminations. Enhancement of charge separation in the PANI/TiO_2 nanocomposite is achieved, because PANI is an efficient electron donor and good hole transporter. These features of PANI lead to the effective separation of photogenerated electron–holes at the interface of PANI and TiO_2 in the nanocomposite (Zhang *et al* 2008; Wang *et al* 2010). Although in this particular molar ratio of TiO_2/PANI (3·79) which was used to prepare PANI/TiO_2 nanocomposite, improvement of PANI/TiO_2 photocatalytic activity under UV light illumination is negligible compared to pristine TiO_2 nanoparticles while, photocatalytic activity of the same composition of PANI/TiO_2 under visible light irradiation is considerably higher than pristine TiO_2 nanoparticles. Also, the obtained regression coefficients suggest the kinetics equation of MeO photodegradation under both UV and visible light illuminations well concisely follow the pseudo-first order reaction kinetics.

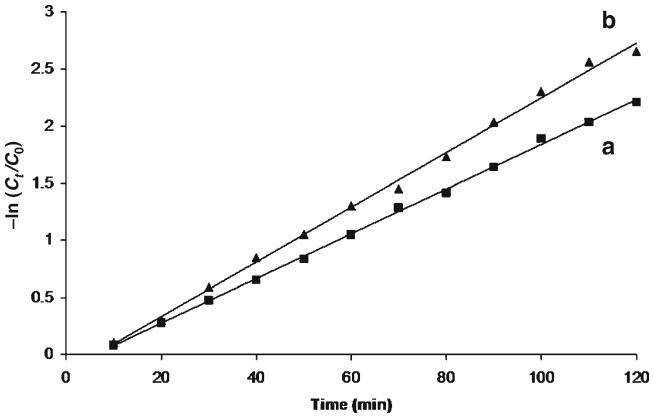

Figure 12. Kinetics plots for linear fitting of data obtained from pseudo-first-order reaction model for MeO degradation under UV light irradiation using pristine TiO_2 (**a**) and PANI/TiO_2 nanocomposite (**b**) as photocatalyst.

Table 2. Apparent rate constants (k_{app}), linear regression coefficients, half time of MeO photodegradation from a plot of $-\ln(C_t/C_0) = k_{app}t$ and degradation efficiency (%) of MeO after 120 min illumination under UV light.

Photocatalyst	Degradation efficiency (%)	R^2	k_{app} (min^{-1})	$t_{1/2}$
Neat TiO_2	89·0	0·998	0·0192	36·09
PANI/TiO_2	92·9	0·996	0·0235	29·49

4. Conclusions

TiO_2 nanoparticles were successfully encapsulated by PANI via *in situ* chemical oxidative polymerization method. Deposition of PANI on the surface of TiO_2 nanoparticles and formation of a core-shell nanocomposite at molecular level were confirmed by FT–IR, UV-Vis-NIR, XRD, SEM and TEM techniques. Results show PANI is a promising material for increasing the photoactivity of TiO_2 nanoparticles under both UV and visible light irradiations. Therefore, surface modification of TiO_2 nanoparticles by PANI via the *in situ* polymerization is a facile method for increasing of the photocatalytic activity of TiO_2 nanoparticles. The PANI/TiO_2 core-shell nanocomposite showed better photocatalytic activity for MeO photodegradation in aqueous solution compared to the pristine TiO_2 nanoparticles under both UV and visible light illuminations.

Acknowledgement

The financial support of this research by the University of Tabriz is gratefully acknowledged.

References

Chen S and Cao G 2006 *Desalination* **194** 127
Chen S and Liu Y 2007 *Chemosphere* **67** 1010
Dey A, De S, De A and De S K 2004 *Nanotechnology* **15** 1277
Dong D, Li P, Li X, Zhao Q, Zhang Y, Jia C and Li P 2010 *J. Hazard. Mater.* **174** 859
Ganesan R and Gedanken A 2008 *Nanotechnology* **19** 435709
Karim M R, Lim K T, Lee M S, Kim K and Yeum J H 2009 *Synth. Met.* **159** 209
Kim B, Lee K, Huh P, Lee D, Jo N and Lee J 2009 *Synth. Met.* **159** 1369
Kosmulski M 2002 *Adv. Colloid Interf. Sci.* **99** 255
Lai C, Zhang H Z, Li G R and Gao X P 2011 *J. Power Sources* **196** 4735
Li G, Zhang D and Yu J C 2009 *Environ. Sci. Technol.* **43** 7079
Li J, Zhu L, Wu Y, Harima Y, Zhang A and Tang H 2006 *Polymer* **47** 7361
Li X Z and Li F B 2001 *Environ. Sci. Technol.* **35** 2381
Li X, Chen W, Bian C, He J, Xu N and Xue G 2003 *Appl. Surf. Sci.* **217** 16
Li X, Wang G, Li X and Lu D 2004 *Appl. Surf. Sci.* **229** 395
Li X, Wang D, Cheng G, Luo Q, An J and Wang Y 2008a *Appl. Catal.* **B81** 267
Li X, Wang D, Luo Q, An J, Wang Y and Cheng G 2008b *J. Chem. Technol. Biotechnol.* **83** 1558
Liao G, Chen S, Quan X, Chen H and Zhang Y 2010 *Environ. Sci. Technol.* **44** 3481
Liao G, Chen S, Quan X, Zhang Y and Zhao H 2011 *Appl. Catal.* **B102** 126
Liu X J and Guo Z P 1991 *Synth. Met.* **41–43** 1139
Lokesh B G, Rao K S V K, Reddy K M, Rao K C and Rao P S 2008 *Desalination* **233** 166
Lu N, Quan X, Li J, Chen S, Yu H and Chen G 2007 *J. Phys. Chem.* **C111** 11836
Min S, Wang F and Han Y 2007 *J. Mater. Sci.* **42** 9966
Mishra P R and Srivastava O N 2008 *Bull. Mater. Sci.* **31** 545
Muktha B, Madras G, Row T N G, Scherf U and Patil S 2007 *J. Phys. Chem.* **B111** 7994
Nagaraja M, Pattar J, Shashank N, Manjanna J, Kamada Y, Rajanna K and Mahesh H M 2009 *Synth. Met.* **159** 718
Narayana R L, Matheswaran M, Aziz A A and Saravanan P 2011 *Desalination* **269** 249
Olad A and Naseri B 2010 *Prog. Org. Coat.* **67** 233
Olad A and Rashidzadeh A 2008 *Prog. Org. Coat.* **62** 293
Polyakov N E, Leshina T V, Meteleva E S, Dushkin A V, Konovalova T A and Kispert L D 2010 *J. Phys. Chem.* **B114** 14200
Pourata R, Khataee A R, Aber S and Daneshvar N 2009 *Desalination* **249** 301
Sakthivel S, Shankar M V, Palanichamy M, Arabindoo B, Bahnemann D W and Murugesan V 2004 *Water Res.* **38** 3001
Salem M A, Al Ghonemiy A F and Zaki A B 2009 *Appl. Catal.* **B91** 59
Sathiyanarayanan S, Azim S S and Venkatachari G 2007 *Electrochim. Acta* **52** 2068
Shi L, Wang X, Lu L, Yang X and Wu X 2009 *Synth. Met.* **159** 2525
Somani P R, Marimuthu R, Mulik U P, Sainkar S R and Amalnerkar D P 1999 *Synth. Met.* **106** 45
Sun Q and Xu Y 2009 *J. Phys. Chem.* **C113** 12387
Wang D P and Zeng H C 2009a *Chem. Mater.* **21** 4811
Wang D P and Zeng H C 2009b *J. Phys. Chem.* **C113** 8097

Wang F and Min S X 2007 *Chin. Chem. Lett.* **18** 1273
Wang F, Min S, Han Y and Feng L 2010 *Superlattices Microstruct.* **48** 170
Wang X, Tang S, Zhou C, Liu J and Feng W 2009 *Synth. Met.* **159** 1865
Xia H and Wang Q 2002 *Chem. Mater.* **14** 2158
Xiong S, Phua S L, Dunn B S, Ma J and Lu X 2010 *Chem. Mater.* **22** 255
Xu J, Liu W and Li H 2005 *Mater. Sci. Eng.* **C25** 444
Yavuz A G and Gok A 2007 *Synth. Met.* **157** 235
Zhang H, Zong R, Zhao J and Zhu Y 2008 *Environ. Sci. Technol.* **42** 3803
Zhang L, Wan M and Wei Y 2005 *Synth. Met.* **151** 1
Zhang L, Liu P and Su Z 2006 *Polym. Degrad. Stab.* **91** 2213
Zhu Y, Xu S and Yi D 2010 *React. Funct. Polym.* **70** 282